Low mechanical loss and high refractive index in amorphous Ta_2O_5 films grown by magnetron sputtering

M. Molina-Ruiz,[1,*] K. Shukla,[2] A. Ananyeva,[3] G. Vajente,[3] M. R. Abernathy,[4,†] T. H. Metcalf,[4] X. Liu,[4] A. Markosyan,[5] R. Bassiri,[6] M. M. Fejer,[6] M. Fazio,[7,‡] L. Yang,[8] C. S. Menoni,[7,8] and F. Hellman[1,2]

[1]*Department of Physics, University of California, Berkeley, Berkeley, California 94720, USA*
[2]*Department of Materials Science and Engineering, University of California, Berkeley, Berkeley, California 94720, USA*
[3]*LIGO Laboratory, California Institute of Technology, Pasadena, California 91125, USA*
[4]*Naval Research Laboratory, Washington, DC 20375, USA*
[5]*Edward L. Ginzton Laboratory, Stanford University, Stanford, California 94305, USA*
[6]*Department of Applied Physics, Stanford University, Stanford, California 94305, USA*
[7]*Department of Electrical and Computer Engineering, Colorado State University, Fort Collins, Colorado 80523, USA*
[8]*Department of Chemistry, Colorado State University, Fort Collins, Colorado 80523, USA*

(Received 2 November 2023; accepted 12 February 2024; published 6 March 2024)

The ability to observe astronomical events through the detection of gravitational waves relies on the quality of multilayer coatings used on the optical mirrors of interferometers. Amorphous Ta_2O_5 (including TiO_2:Ta_2O_5) currently limits detector sensitivity due to high mechanical loss. In this paper, mechanical loss measured at both cryogenic and room temperatures of amorphous Ta_2O_5 films grown by magnetron sputtering and annealed in air at 500 °C is shown to decrease for elevated growth temperature. Films grown at 310 °C and annealed yield a mechanical loss of 3.1×10^{-4} at room temperature, the lowest value reported for pure amorphous Ta_2O_5 grown by magnetron sputtering to date, and comparable to the lowest values obtained for films grown by ion beam sputtering. Additionally, the refractive index n increases 6% for elevated growth temperature, which could lead to improved sensitivity of gravitational-wave detectors by allowing a thickness reduction in the mirrors' coatings. Structural characterization suggests that the observed mechanical loss reduction in amorphous Ta_2O_5 films with increasing growth temperature correlates with a reduction in the coordination number between oxygen and tantalum atoms, consistent with TaO_x polyhedra with increased corner-sharing and reduced edge- and face-sharing structures.

DOI: 10.1103/PhysRevMaterials.8.035603

I. INTRODUCTION

The detection of gravitational waves (GWs) relies on the precise measurement of the optical phase difference between two light beams from a common source traveling back and forth between mirrors in the perpendicular arms of an interferometer [1,2]. The optimal performance of these mirrors is achieved by the use of Bragg mirrors, which yield high reflectivity and low optical absorption, and consist of alternating low- and high-refractive index n amorphous dielectric layers [3]. Thermal noise, a type of energy dissipation and currently the dominant source of noise in these mirrors, originates in the coatings of the intermeformeter mirrors and is the factor that limits the sensitivity of GW detectors, such as the Laser Interferometer Gravitational-Wave Observatory (LIGO), Virgo, and the Kamioka Gravitational Wave Detector (KAGRA) interferometers [4,5].

The large dimensions of the mirrors used in GW detectors favors the use of amorphous (a-)coatings, specifically, amorphous silica a-SiO_2 (as the low n layer) and amorphous tantala a-Ta_2O_5 or titania-doped tantala a-TiO_2:Ta_2O_5 (as the high n layer) for KAGRA or LIGO and Virgo, respectively. The high n layer contributes more to the overall thermal noise of the mirrors [6]. The lack of long-range order in amorphous materials enables additional dissipation mechanisms, such as in mechanical loss, that increase the mirrors' thermal noise [4]. At low temperatures, below ∼10 K, mechanical loss is well described by the standard tunneling model [7,8], in which groups of atoms tunnel between nearby configurations with similar energies, i.e., two-level systems (TLSs) in their most simplified mathematical expression [9]. At higher temperatures, TLSs become thermally activated and the transition between states happens by jumping over the energy barriers that separate different states [10]. It was found that a-TiO_2 reduces the loss to 2×10^{-4} upon incorporation in the a-Ta_2O_5 network [11]. However, a deeper understanding of the connection between loss mechanisms and structure of a-Ta_2O_5 will better guide further and improved versions of GW detectors.

Previous results show that elevated growth temperature reduces the mechanical loss due to tunneling (<10 K) of amorphous silicon [12,13], as well as the mechanical loss

*Corresponding author: manelmolinaruiz@gmail.com
†Present address: The Johns Hopkins University Applied Physics Laboratory, Laurel, Maryland 20723, USA.
‡Present address: University of Strathclyde, Glasgow, G1 1XQ, United Kingdom.

due to thermally activated processes at room temperature of a-Ta_2O_5 films grown by both magnetron sputtering (MS) and ion beam sputtering (IBS) [14]. It has also been shown that the thermally activated mechanical loss of MS a-Ta_2O_5 films, which is important above 100 K, *increases* with higher annealing temperatures [15]. Previous work explored different ways to reduce the mechanical loss at room temperature of a-Ta_2O_5 films for GW detectors [16–19].

In this paper, we present a comprehensive study of structural, elastic, and optical properties of pure a-Ta_2O_5 films grown by reactive DC MS. We report the effects of growth temperature and annealing at various temperatures on atomic density, surface roughness, and film strain, Raman-derived structural properties, refractive index, and extinction coefficient, mechanical loss measured at cryogenic and room temperatures, and shear and Young's modulus.

II. EXPERIMENTAL METHODS

Amorphous Ta_2O_5 films ∼600 nm thick were grown by reactive (80% Ar+20% O_2 mixed gas) MS from a 99.95% pure tantalum target, with the substrate temperature T_S at 50, 160, 310, and 460 °C, chosen to be below 480 °C at which prior work on MS a-Ta_2O_5 has shown crystallization [14]. The chamber base pressure was $<8 \times 10^{-8}$ Torr. During growth, the working gas pressure was maintained at 7.25 mTorr with a flow rate of 2 sccm pure O_2 (99.99%) introduced at the substrates and 8 sccm pure Ar (99.998%) introduced at the Ta target. The power at the tantalum source was maintained at 120 W with 380 V. In comparison to the previously studied a-Ta_2O_5 films grown by MS [14], the films reported in this paper are grown at higher pressure, lower power, and lower rate. A quartz crystal monitor was used to monitor the growth rate, which was ∼1.0 Å/s. Annealing was performed *ex situ* in air at either 500 or 600 °C for 3 h. As grown, films were found to be near the desired stoichiometry (0.8 at. % O below the desired 71.4 at. % O) and nearly transparent for room-temperature growth, but increasing growth temperature led to somewhat opaque films with up to 3 at. % O below stoichiometry (see details in Supplemental Material [20]). Annealing in air enables oxygen to diffuse [14] and led to full transparency and improved stoichiometry (within ±0.3 at. % of the desired Ta_2O_5 composition) for all growth temperatures. The films showed the crystallization onset after annealing at 700 °C (no crystallization was observed for films annealed at 650 °C).

Structural, optical, and acoustic measurements were performed on all samples after annealing at different temperatures. Films for structural, optical, and acoustic characterizations were grown on either crystalline silicon, with the native oxide layer left intact, or silica substrates, as will be described below.

A. Structural characterization

Parallel beam x-ray diffraction (PB-XRD) was used to look for crystallinity in the a-Ta_2O_5 films. Traditional x-ray diffraction (XRD) techniques use Bragg-Brentano geometry, which gives high resolution and high beam intensity analysis at the cost of requiring precise alignment of the coordinate position and angle of the sample. Misalignment of films, surface roughness, and a lack of clear crystalline directions lead to error and noise in XRD measurements. The grazing incidence angle of the PB-XRD experimental setup maximizes the signal from the film and minimizes substrate signal interference. Additionally, the parallel beam allows a larger surface of the sample to be probed, thereby reducing the noise from surface roughness. The PB-XRD employs an Cu K_α x-ray beam of 1.54 Å and continuously scans between 2θ values of 10.00°and 60.00° with a step size of 0.01° and step time of 0.25 seconds.

Rutherford backscattering spectrometry (RBS) was used to determine the stoichiometry and the areal density depth profile of the a-Ta_2O_5 films. Elastic recoil detection analysis (ERDA) was used to quantify the hydrogen within the films. RBS and ERDA were performed in a NEC model 5SDH Pelletron tandem accelerator, with α particles beam energy tuned to show oxygen resonance at the surface of the films (∼3 MeV). The thickness of the films was measured by profilometry using a KLA-Tencor Alpha-Step IQ profilometer. RBS and profilometry measurements were combined to obtain the atomic density and from that the mass density of the a-Ta_2O_5 films.

Raman spectroscopy was performed using a Renishaw inVia with a 488 nm 488 nm argon-neon laser linearly polarized to probe the local bonding environment. The substrate background was subtracted based on a bare substrate measurement (accounting for the intensity reduction after the laser goes through the film).

A Digital Instruments Dimension 3100 atomic force microscope was used to measure the roughness and topography of the a-Ta_2O_5 films.

Substrate curvature measurements were taken using a Tencor FLX-2320 thin-film stress instrument to measure the macroscopic stress within the films and their corresponding strain. The stress was obtained using Stoney's equation [22] with no corrections, since the thickness ratio for the tantala films grown on 100-μm-thick crystalline silicon wafers is $0.006 \ll 1$ [23], which allowed the assumption that all strain is accommodated in the film. The macroscopic strain therefore is given by $\varepsilon = -\sigma_i(1-\nu)/E$, where σ_i and E are the measured internal stress and Young's modulus of the film, respectively, and $\nu = E/2G - 1$ is the Poisson's ratio determined from the measured values of E and G, where G is the shear modulus. The measured total stress σ is corrected by the thermal stress σ_{th} induced when the film preparation and the substrate curvature measurement are done at different temperatures. The film internal stress σ_i is given by

$$\sigma_i = \sigma - \sigma_{\text{th}} = \sigma - E(\alpha_f - \alpha_s)(T_S - T_M), \qquad (1)$$

where $\alpha_f = 3.6 \times 10^{-6}\ ^\circ\text{C}^{-1}$ [24] and $\alpha_s = 2.6 \times 10^{-6}\ ^\circ\text{C}^{-1}$ [25] are the film and substrate thermal expansion coefficients, respectively, and T_M is the temperature at which the substrate curvature is measured.

B. Optical characterization

The refractive index n and extinction coefficient k of the a-Ta_2O_5 films were determined by measuring light intensity and its phase in reflection and transmission for an incident angle of 60° using a Horiba UVISEL ellipsometer in a spectral

range of 0.64 eV to 4.50 eV, with a resolution of 0.01 eV. The analysis of the phase shift of the light beam traveling through the a-Ta_2O_5 film was performed using the DeltaPsi2 software and a Cody-Lorentz optical model [26]. The films were deposited on 2-in.-diameter fused silica wafers 0.5 mm thick.

C. Acoustic characterization

The mechanical loss and elastic moduli of the films was determined through the energy dissipation caused by atomic motion in the films, which is measured by determining the ring-down time of two different types of resonators: a double-paddle oscillator (DPO) and a gentle nodal suspension (GeNS) system.

1. Double-paddle oscillator

The DPO technique measures the films' transverse (shear) acoustic properties as a function of temperature, specifically both dissipative loss and shear modulus. Films were deposited on DPOs, butterfly-winged high-resistivity 300-μm-thick (100) crystal silicon devices, which measure, through the shift in the devices' resonant frequency, the shear modulus G and the transverse mechanical loss $Q^{-1}(T)$ in the temperature range from 300 mK to 120 K [27]. The error associated to Q^{-1} measurements is ∼5%. Each DPO was annealed at 450 °C under vacuum and measured prior to deposition to give an accurate background loss and shear modulus [28]. The high values of the quality factor of the bare DPO ($Q \sim 1 \times 10^8$), obtained for the second antisymmetric vibrational mode at ∼5500 Hz, provides high mechanical loss and resonance frequency sensitivity [29,30].

2. Gentle nodal suspension

The GeNS technique used in this paper determines the Young's modulus E and mechanical loss at room temperature Q_{RT}^{-1} [31]. The films were deposited on 2-in.-diameter fused silica wafers 0.5 mm thick, then measured at several frequencies (between 500 Hz and 33 kHz) that have both shear and bulk mode contributions [32]. Prior to deposition, the wafers were annealed at 900 °C to improve their quality factor Q and measured to determine their loss background [14].

III. RESULTS

The as-deposited a-Ta_2O_5 films showed a gray coloration, which was shown by RBS measurements to be due to oxygen deficiency in the films and ranged from 0.8 at. % O, for films grown at 50 °C, to 3.0 at.% O, for films grown at 460 °C (see further details in the Supplemental Material [20]). After annealing at 500 °C in air for 3 h, the films became completely transparent, with a density of 7.4 ± 0.2 g/cm^3 and RBS confirmed that the desired 2:5 stoichiometry (within 0.3 at. % O, the limit of the RBS resolution) was achieved [20]. The density of our films after annealing at 500 °C is compatible with previously reported values of annealed a-Ta_2O_5 films grown by MS and IBS, which range from 7.3 to 7.8 g/cm^3 [14,33,34]. No further changes were observed in the transparency or stoichiometry of the films after additional annealing at 600 °C in air for 3 h.

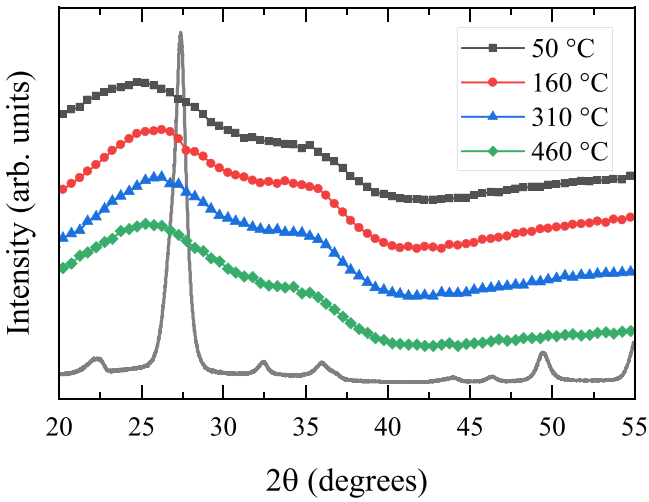

FIG. 1. PB-XRD results for a-Ta_2O_5 films grown at the temperatures shown in the legend after annealing in air at 600 °C for 3 h. Crystalline tantala (grey line) from Ref. [32] is shown for comparison. All spectra have been vertically shifted for readability purposes.

Annealed films showed small amounts of Ar and H incorporation: up to 1 at. % Ar and up to 3.4 at.% H. Argon is commonly incorporated into films grown by sputtering [35,36], and the ⩽ 1 at. % Ar seen in these films is relatively low and comparable to other a-Ta_2O_5 films also grown by MS [37]. Hydrogen can be incorporated into the films during growth due to gas impurities, and also after growth through water absorption from air. In this paper, we did not perform ERDA on capped films, which can absorb hydrogen during growth but not after exposure to air via water molecules, and therefore we cannot quantify the at. % H from each process. The atomic hydrogen concentration in the as-deposited a-Ta_2O_5 films reduces with increasing growth and annealing temperatures [20]; in films grown from 50 to 460 °C and annealed at 500 °C, it reduces from 3.4 to 0.6 at. % H, respectively. Subsequent annealing at 600 °C further reduces the hydrogen concentration an additional ∼25%. The films' stoichiometry values previously discussed are obtained, assuming that hydrogen atoms are not bonded to oxygen atoms. It is also possible that some of the hydrogen atoms are forming water molecules, and therefore some of the oxygen detected by RBS belongs to water rather than to the a-Ta_2O_5 films. The stoichiometry values, shown in detail in the Supplemental Material [20], can be adjusted considering that a fraction of the hydrogen atoms are forming water molecules. In this case, the annealed films show an oxygen deficiency up to 0.5 at. % O when grown at 50 °C, and up to 0.1 at. % O when grown at 460 °C.

A. Structural properties

The XRD results presented in Fig. 1 show that a-Ta_2O_5 films grown up to 460 °C are amorphous even after being annealed at 600 °C, which has been observed for a-Ta_2O_5 films grown by IBS [38]. We observe two broad features centered around 26°and 35°. Similar results were reported for other MS a-Ta_2O_5 films grown up to 400 °C [14].

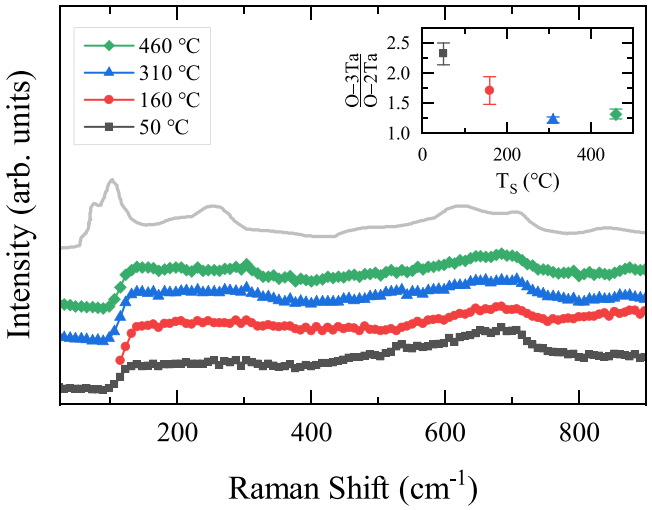

FIG. 2. Raman spectra of samples annealed at 600 °C. For comparison, the Raman spectra of crystalline β-Ta_2O_5 (grey line) is shown [40]. All spectra have been vertically shifted for readability purposes. Inset: The ratio of O–3Ta and O–2Ta bonds as a function of growth temperature T_S. The bond ratio is obtained from the intensities of the Raman features shown in the main figure as described in the text.

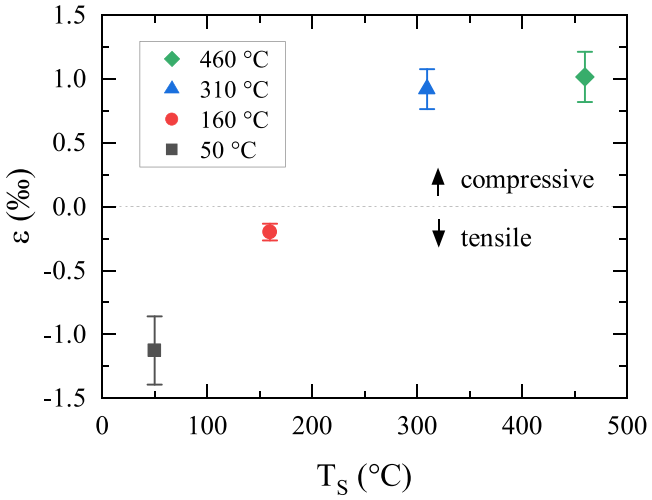

FIG. 3. Strain ε of a-Ta_2O_5 films annealed at 600 °C as a function of growth temperature T_S. The quantities used to determine the strain given by $\varepsilon = -\sigma_i(1-\nu)/E$, are σ_i that is obtained from wafer curvature measurements, and ν and E that are obtained from acoustic property measurements (see Sec. III C 2). Black arrows show the regions of compressive ($\sigma_i < 0$) and tensile ($\sigma_i > 0$) stress.

The RMS surface roughness R_q of the a-Ta_2O_5 films, annealed at 500 °C, decreases from 3.4 nm to 1.8 nm with increasing growth temperature.

Figure 2 shows the Raman spectra of 600 °C annealed a-Ta_2O_5 films grown at different temperatures, along with the spectrum for crystalline Ta_2O_5. The significant observable features have been associated with specific bond deformations [39]. The broad plateau observed from 100 to 300 cm^{-1} corresponds to bending and rocking vibrations of O–2Ta bonds (oxygen atoms bonded to two tantalum atoms each), and increases its intensity with increasing T_S. The peak observed at ∼680 cm^{-1} corresponds to the bending and stretching of O–3Ta bonds (oxygen atoms bonded to three tantalum atoms each), and reduces its intensity as T_S increases. The inset in Fig. 2 shows that the ratio of intensities between the ∼680 cm^{-1} peak and the 100 to 300 cm^{-1} broad plateau, i.e., the intensities associated with O–3Ta and O–2Ta bonds, decreases with increasing growth temperature. These observations therefore suggest that films grown at higher temperatures show an increase of O–2Ta bonds, and a reduction of O–3Ta bonds.

The apparent lack of correlation between Raman spectra for amorphous and crystalline Ta_2O_5, shown in Fig. 2, is caused by changes in the phonon density of states combined to the breaking of the Raman selection rules in the amorphous phase [40]. Differences between the amorphous and crystalline structures originate in their short-range order due to fluctuations in the interatomic distances and coordination numbers of TaO_x polyhedra [41,42]. In the crystalline structure, these polyhedra are organized systematically providing long-range order. In the amorphous counterpart, the small differences in shape and random orientation of the polyhedra described above cause variations in medium-range order and the loss of long-range order [39,43].

The substrate curvature measurements (corrected for differential thermal contraction, as described in Sec. II A) provide the strain of annealed films at room temperature and how it depends on growth temperature. Figure 3 shows that films grown at 50 °C exhibit tensile strain, which is reduced with increasing growth temperature. We observe a crossover to compressive strain for films grown at 310 °C and higher. The differential thermal contraction between substrate and films that are grown above room temperature has a moderate effect on the measured films strain; we quantify a thermal strain of −0.11, −0.23, and −0.35%, for films grown at 160, 310, and 460 °C, respectively.

B. Optical properties

The index of refraction n and the extinction coefficient k of a-Ta_2O_5 films are shown in Figs. 4(a) and 4(b), respectively. Figure 4(a) shows n from 0.64 to 4.50 eV for films grown at various growth temperatures and annealed at 500 °C. At 1.2 eV (1064 nm), the energy at which LIGO, Virgo, and KAGRA presently operate, n increases from 2.08 to 2.21 with T_S, more than a 6% increase. Other a-Ta_2O_5 films grown by IBS at room temperature and annealed at 500 °C report n values ranging from 2.03 to 2.09 [19,34], consistent with our results.

Figure 4(b) shows k from 0.64 to 4.50 eV for the same films. Below 3.4 eV for the films grown at 460 °C, and below 3.7 eV for all other films, $k < 10^{-4}$, which implies that the optical absorption of these films is low. However, our technique does not have enough resolution to determine the optical absorption in parts per million of these films. The optical band gap E_g of the a-Ta_2O_5 films is determined from linear fits of the high-energy range of the Tauc plot shown in the inset of Fig. 4(b). Despite the observed changes in n with growth temperature, E_g does not notably change within the accuracy of the technique and has a value of 4.0 ± 0.1 eV,

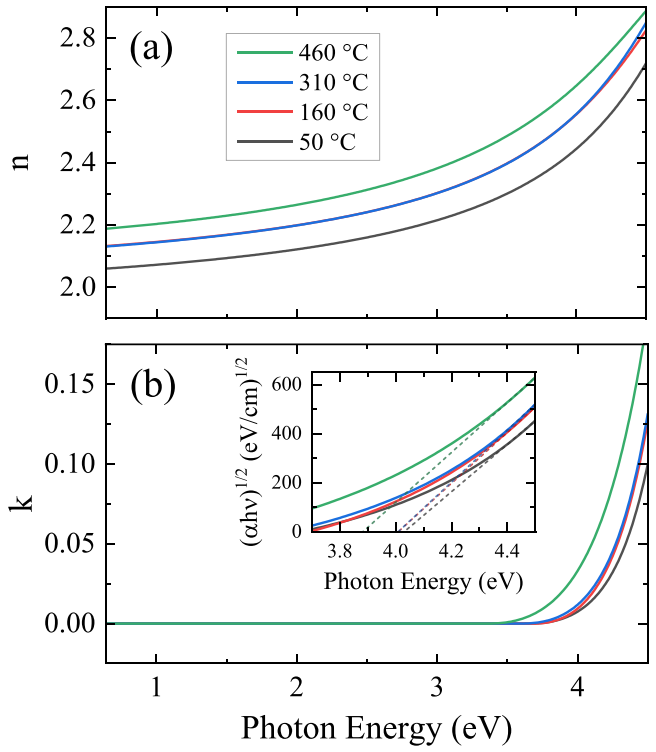

FIG. 4. (a) Index of refraction n and (b) extinction coefficient k as a function of photon energy for a-Ta_2O_5 films deposited at 50 °C (black lines), 160 °C (red lines), 310 °C (blue lines), and 460 °C (green lines), and annealed at 500 °C. Note that in (a), n for 160 and 310 °C films are nearly the same. Inset in (b) shows a Tauc plot of the same films showing $(\alpha h\nu)^{1/2}$ vs energy, where α is the absorption coefficient and $h\nu$ the photon energy. The dashed black lines are linear fits used to determine the optical band gap E_g of the films.

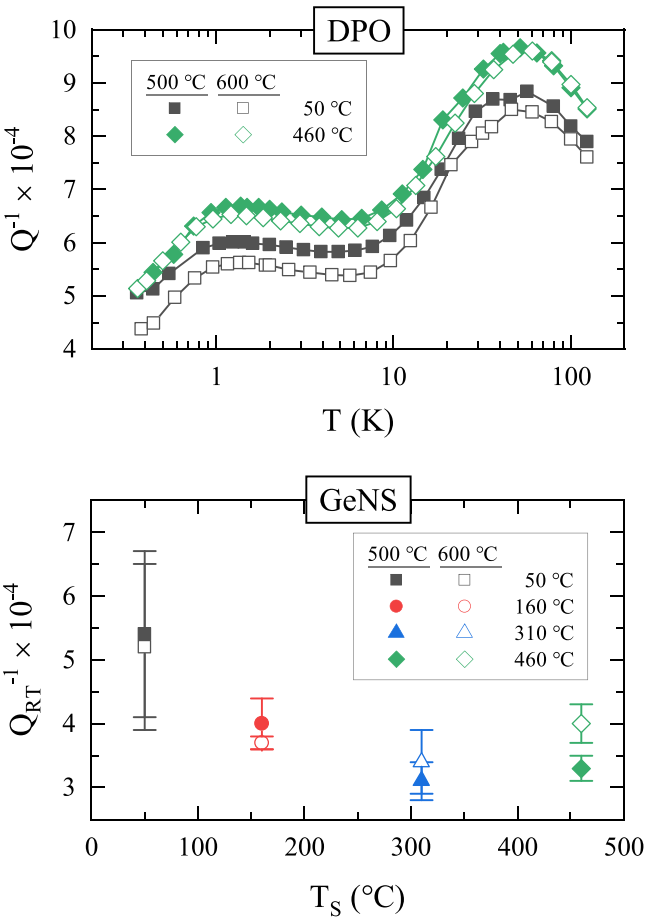

FIG. 5. Mechanical loss Q^{-1} of a-Ta_2O_5 films grown at 50 °C (black squares), 160 °C (red circles), 310 °C (blue triangles), and 460 °C (green diamonds), annealed at 500 °C (closed symbols) and at 600 °C (open symbols). Top panel: Q^{-1} as a function of measurement temperature T using DPO technique. Bottom panel: Q_{RT}^{-1} as a function of substrate temperature T_S measured at room temperature using GeNS technique, where each Q^{-1} data point is obtained by averaging measurements done between 500 Hz and 33 kHz.

in agreement with $E_g = 4.0$ eV obtained for other amorphous tantala films grown by MS [44,45], and similar to IBS films that range from 4.0 to 4.3 eV [46,47]. The slight reduction in E_g for films grown at 460 °C, as opposed to those grown at lower temperatures, may be attributed to subtle structural variations, potentially observable in the Raman results shown in Fig. 2, or compositional distinctions below the 0.3 at. % resolution for oxygen.

C. Acoustic properties

1. Mechanical loss

Figure 5 shows the mechanical loss, from 0.3 to 120 K, Q^{-1} of a-Ta_2O_5 films as a function of measurement temperature T (measured by DPO), and the mechanical loss, at room temperature, Q_{RT}^{-1} of a-Ta_2O_5 films as a function of growth temperature T_S (measured by GeNS). Q^{-1} decreases, on average over the measured temperature range, 7% and 2% with increasing annealing temperature for films grown at 50 and 460 °C, respectively. This reduction is systematic but within errors. Q_{RT}^{-1} decreases with increasing annealing temperature for samples grown at 50 and 160 °C, and increases for samples grown at 310 and 460 °C. Changes in Q_{RT}^{-1} with increasing annealing temperature, however, are within errors except for the film grown at 460 °C.

The mechanical loss Q^{-1} between 1 and 10 K (top panel in Fig. 5), where energy dissipation is due to tunneling [9], is lower for films grown at 50 °C, for both 500 and 600 °C annealed states, with a lowest value of 5.5×10^{-4} for the a-Ta_2O_5 film grown at 50 °C and annealed at 600 °C. At room temperature (bottom panel in Fig. 5), where energy dissipation is due to thermal activation [48], Q_{RT}^{-1} decreases with increasing T_S, with a lowest value of 3.1×10^{-4} for a-Ta_2O_5 film grown at 310 °C and annealed at 500 °C. This is the lowest value measured at room temperature for pure a-Ta_2O_5 films grown by MS, and comparable to a-Ta_2O_5 films grown by IBS [14]. Figure 5 shows a crossover in the mechanical loss with growth temperature, i.e., Q^{-1} is lower (higher) for films grown at lower (higher) temperature while Q_{RT}^{-1} is lower (higher) for films grown at higher (lower) temperature. Previous work reported a similar crossover in the mechanical loss of a-Ta_2O_5 films with annealing temperature [15,49].

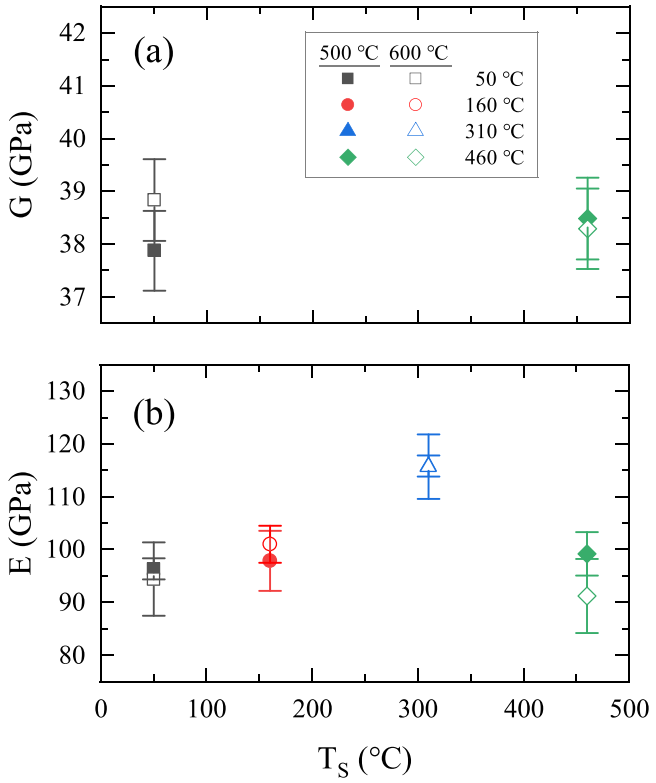

FIG. 6. (a) Shear modulus G and (b) Young's modulus E of a-Ta_2O_5 films annealed at 500 °C (closed symbols) and at 600 °C (open symbols), as a function of growth temperature T_S. Data shown was measured at 300 K by DPO (a) and GeNS (b). DPO data shows that G increases slightly with decreasing measurement temperature (<5% at 1 K).

The mechanical loss at room temperature Q_{RT}^{-1} of films deposited at 460 °C and annealed is slightly larger than that of films deposited at 310 °C and annealed, as already reported in previous studies of a-Ta_2O_5 films [14].

2. *Elastic properties*

The shear modulus G and Young's modulus E of the a-Ta_2O_5 films measured by DPO and GeNS is shown in Figs. 6(a) and 6(b), respectively, as a function of growth temperature (after annealing at 500 and 600 °C). G and E do not show any significant variation with annealing temperature. For all films, G is 38 to 39 GPa and E varies between 91 to 116 GPa. We experimentally determine the Poisson's ratio of the films grown at 50 and 460 °C using the relationship $\nu = E/2G - 1$, and obtain 0.28 ± 0.03 and 0.21 ± 0.07 for the a-Ta_2O_5 films annealed at 500 and 600 °C, respectively. These results are comparable to the Young's modulus value of 118 GPa and the Poisson's ratio value of 0.28 reported for IBS a-Ta_2O_5 films [19].

IV. DISCUSSION

In this paper, a-Ta_2O_5 films are grown by reactive DC MS using lower energy incident atoms (lower power and higher working gas pressure) in comparison to previous work [14,19]. Under these conditions, the energy of the atoms

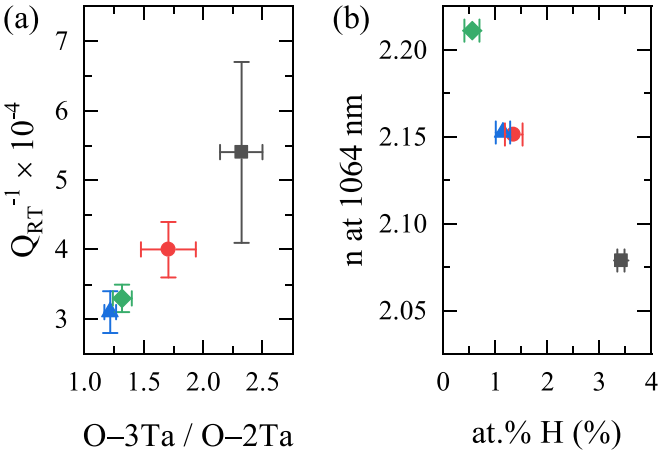

FIG. 7. (a) Mechanical loss at room temperature Q_{RT}^{-1} as a function of the ratio between O–3Ta and O–2Ta bonds. (b) Refractive index n at 1064 nm as a function of hydrogen concentration at. % H. Both plots show data from a-Ta_2O_5 films grown at 50 °C (black squares), 160 °C (red circles), 310 °C (blue triangles), and 460 °C (green diamonds), and annealed at 500 °C.

arriving at the substrate is significantly reduced by collisions with Ar atoms at these higher gas pressures, resulting in less densification and less subsurface damage [50,51]. The reduced energy gives molecules and atoms adsorbed on the film surface time to diffuse and find lower energy equilibrium positions with increasing growth temperature. By contrast, with higher energy atoms, growth temperature is less important [52]. The decreased incident energy prevents subsurface embedding, and elevated substrate temperature further increases the surface diffusion of adatoms and molecules on the surface of the film.

a-Ta_2O_5 films prepared by MS grown at 310 °C and subsequently annealed at 500 °C in air yield a mechanical loss at room temperature of 3.1×10^{-4}, which is comparable to the lowest value of $(2.7 \pm 0.8) \times 10^{-4}$ measured for films grown by IBS, and 30% lower than the previous lowest loss for a-Ta_2O_5 films grown by MS [14]. Therefore, high n films, those used in LIGO, Virgo, and KAGRA GW detectors, prepared under these conditions could potentially further reduce the detectors' thermal noise. These results demonstrate that lower power and higher gas pressure, both of which cause the adatoms to have lower kinetic energy, is more effective at producing films with lower mechanical loss than room-temperature growth at higher power and lower gas pressure, which cause higher adatom kinetic energy. Elevated growth temperature further enhances the ability of MS to produce a-Ta_2O_5 films with lower Q_{RT}^{-1}. By contrast, Fig. 5(a) shows that Q^{-1}, and specifically the plateau Q_0^{-1} where tunneling dominates, increases with increasing growth temperature, and decreases slightly with increased annealing temperature.

Raman characterization shows that higher growth temperature yields a-Ta_2O_5 films with increased O–2Ta bonds, and reduced O–3Ta bonds. Corner-sharing structures in a-Ta_2O_5 have been associated with O–2Ta bonds, while edge- and face-sharing structures have been associated with O–3Ta bonds [53]. Therefore, our results in Fig. 7(a) show that the reduction of edge- and face-sharing structures and the increase in

corner-sharing structures, i.e., the reduction of the coordination number between oxygen and tantalum atoms, correlates with the reduction of Q_{RT}^{-1} in a-Ta_2O_5 films. Prasai *et al.* [54] measured the mechanical loss and the pair distribution function of zirconia-doped tantala films and found that Q_{RT}^{-1} correlated with face- and edge-sharing polyhedra, while Q^{-1} below 120 K was dominated by corner-sharing polyhedra. Since the ratio of these types of polyhedra must obey a sum rule, the decrease in Q_{RT}^{-1}, e.g., with growth temperature, would be accompanied by the increase in Q^{-1} below 120 K, and vice versa. In the present paper, we provide further evidence that this correlation is supported.

Perhaps most significantly, growth temperature has a noticeable effect on the refractive index n and the extinction coefficient k measurements on annealed a-Ta_2O_5 films. It is remarkable that n increases with increasing growth temperature even after annealing at 500 or 600 °C. This result cannot be explained by changes in stoichiometry nor by an increase in density (within the resolution limits of the techniques used); in the annealed state, all films are completely transparent, the RBS measurements yield the expected 2:5 ratio between Ta and O atoms, and their mass density is independent of growth temperature [20]. This result, however, could be explained by the reduction in hydrogen concentration at. % H as growth temperature increases. It has been shown that the refractive index of silicon dioxide decreases as the hydrogen content in the films increases [55]; perhaps hydrogen has a similar effect in tantalum pentoxide films. Our results in Fig 7(b) show an inverse correlation between n and at. % H as the growth temperature increases. Increased growth temperature is responsible for the reduction in at. % H, but the correlation between n and at. % H is stronger than that between n and T_S, seen most clearly in the growths at 160 and 310 °C, where both n and at. % H do not change. Similarly, while the ratio of O–3Ta to O–2Ta bonds and Q_{RT}^{-1} also both depend on growth temperature, they are nonmonotonic in T_S, such that the correlation between these two is much stronger than the correlation with growth temperature, and the correlation of either of these with n or at. % H is poor.

For years, there has been speculation that mechanical loss may be influenced by local strain, which modifies the barrier height or potential well asymmetry of TLSs. This local strain arises from atomic changes in the lattice structure, and some experimental evidence of its effect on mechanical loss has been reported [56]. Our results shown in Fig. 8(a) show a correlation between macroscopic strain and mechanical loss at room temperature, in which Q_{RT}^{-1} decreases as the strain within the films increases, i.e., as the strain changes from tensile to compressive. We also note a similar and perhaps surprising correlation between macroscopic strain and O–3Ta and O–2Ta bonds, shown in Fig. 8(b), in which the ratio of bonds decreases as the strain increases. We suggest that the correlation seen in Fig. 8(a) reflects an underlying correlation of Q_{RT}^{-1} with bond ratio, shown in Fig. 7(a), and that the correlation between Q_{RT}^{-1} and strain seen in Fig. 8(a) is caused by the effect of the macroscopic strain on the bond ratio seen in Fig. 8(b). We note again that the bond ratio can be directly related to the fraction of face- and edge-sharing to corner-sharing polyhedra discussed in Ref. [54].

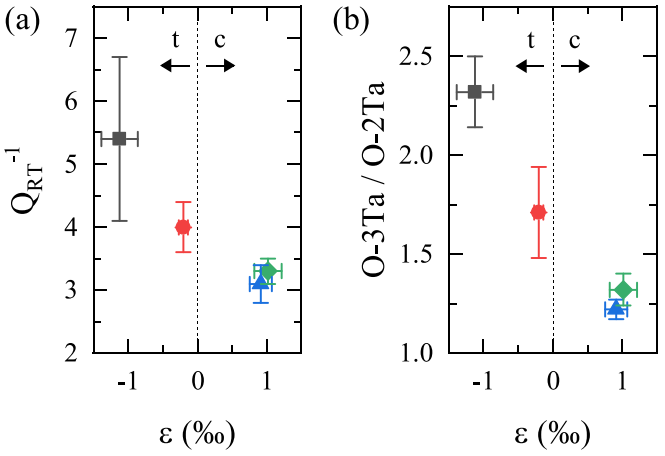

FIG. 8. (a) Mechanical loss at room temperature Q_{RT}^{-1} and (b) ratio of O–3Ta to O–2Ta bonds, both as a function of film macroscopic strain ε for films grown at 50 °C (black square), 160 °C (red circle), 310 °C (blue triangle), and 460 °C (green diamond). Black arrows show the regions of tensile (t) and compressive (c) stress.

The GW detectors' thermal noise is proportional to the total thickness of the coating, which implies that a GW detector with thinner coatings has lower thermal noise and, therefore, enhanced sensitivity. Our results show an increase in n by ∼6% with increased growth temperature, which allows for a similar reduction in thickness, and hence a significant decrease of the GW detectors' thermal noise. Recent work shows that n increases by adding titania to tantala [57], which effectively reduces the thermal noise by decreasing the necessary number of layers, but the idea of increasing n by growth conditions has not yet been explored by the GW community. These results thus present a strategy not explored by the GW community yet to improve the resolution of GW detectors, albeit with the significant cost of growth at elevated temperature. The largest increase in n was seen for films deposited at 460 °C, but even films deposited at 160 °C showed a ∼4% increase at 1064 nm.

Previous work on a-Ta_2O_5 films, grown by both MS and IBS at different temperatures, reported that after annealing, Q_{RT}^{-1} does not depend on growth temperature [14], i.e., that the growth history is eliminated after annealing. In this paper, by contrast, we show that increased growth temperature improves the properties (increases n and reduces Q_{RT}^{-1}) of annealed films. After annealing at 600 °C, Q^{-1} decreases for a-Ta_2O_5 films grown at 50 and 460 °C, while Q_{RT}^{-1} decreases for films grown at 50 and 160 °C, and increases it for films grown at 310 and 460 °C. These variations, however, are within errors for films grown at all temperatures except for the Q_{RT}^{-1} of films grown at 460 °C. We also observe that higher growth temperature yields a-Ta_2O_5 films with *higher* Q^{-1} below 120 K, contrary to what was previously observed in our work in MS a-Si and evaporated a-Ge, where higher growth temperature yields films with lower Q^{-1} from 0.3 to 100 K [58,59].

V. CONCLUSIONS

We have studied the structural, optical, and acoustic properties of amorphous tantala films prepared by reactive DC MS

and grown and annealed at various temperatures. Compared to prior work on tantala, the *a*-Ta_2O_5 films presented in this paper are grown with lower energy of adatoms, which causes growth temperature to matter more. Annealed films measured at room temperature show increasing refractive index and decreasing mechanical loss with increasing growth temperature. Mechanical loss measured at cryogenic temperatures, however, increases with higher growth temperature. Differences in films' strain, corner-, edge- and face-sharing structures, refractive index, and mechanical loss due to increased annealing temperature are small compared to their differences due to increased growth temperature. Mechanical loss results correlate with Raman data on the ratio of O–3Ta to O–2Ta bonds, which are related to the fraction of face- and edge-sharing to corner-sharing polyhedra.

Contrary to commonly held belief, annealing does not always eliminate the material growth history; the lowest mechanical loss, the highest shear, and Young's moduli, and an increase in the refractive index reported in this paper are found for *a*-Ta_2O_5 films grown at 310 °C and subsequently annealed in air at 500 °C. Significant improvement is found even in films grown at 160 °C relative to those grown at 50 °C, which may be important for commercial coating systems, although noting that higher energy growth systems such as IBS may be less impacted by growth temperature than MS. These results suggest that the high refractive index layer used in LIGO, Virgo, and KAGRA GW detectors, could be further improved to reduce the detectors' thermal noise and, therefore, to improve their sensitivity. This improvement may be achieved if IBS *a*-TiO_2:Ta_2O_5 films can be prepared with a lower ratio of O–3Ta to O–2Ta bonds, leading to *lower* mechanical loss, and with a lower hydrogen concentration, leading to *higher* refractive index.

ACKNOWLEDGMENTS

The authors thank P. Ci and J. Wu for assistance with Raman measurements. We gratefully acknowledge support of the LIGO Scientific Collaboration (LSC) Center for Coatings Research (CCR), jointly funded by the United States National Science Foundation (NSF) through Grants No. PHY-2011719, No. 2011571, No. 2011706, No. 1708010, No. 1710957, No. 0823459, and No. 0757058 to each institution, and the Gordon and Betty Moore Foundation through Grant No. 6793. This work was also partially supported by the Office of Naval Research at NRL.

[1] B. P. Abbott, R. Abbott, T. D. Abbott, M. R. Abernathy, F. Acernese, K. Ackley, C. Adams, T. Adams, P. Addesso, R. X. Adhikari *et al.* (LIGO Scientific Collaboration and Virgo Collaboration), Phys. Rev. Lett. **116**, 131103 (2016).

[2] B. P. Abbott, R. Abbott, T. D. Abbott, M. R. Abernathy, F. Acernese, K. Ackley, C. Adams, T. Adams, P. Addesso, R. X. Adhikari *et al.* (LIGO Scientific Collaboration and Virgo Collaboration), Phys. Rev. Lett. **116**, 061102 (2016).

[3] J. Steinlechner, Phil. Trans. R. Soc. A **376**, 20170282 (2018).

[4] Y. Levin, Phys. Rev. D **57**, 659 (1998).

[5] A. E. Villar, E. D. Black, R. DeSalvo, K. G. Libbrecht, C. Michel, N. Morgado, L. Pinard, I. M. Pinto, V. Pierro, V. Galdi, M. Principe, and I. Taurasi, Phys. Rev. D **81**, 122001 (2010).

[6] J. Aasi, B. P. Abbott, R. Abbott, T. D. Abbott, M. R. Abernathy, K. Ackley, C. Adams, T. Adams, P. Addesso, R. X. Adhikari *et al.*, Class. Quantum Grav. **32**, 074001 (2015).

[7] P. W. Anderson, B. I. Halperin, and C. M. Varma, Philos. Mag. **25**, 1 (1972).

[8] W. A. Phillips, J. Low Temp. Phys. **7**, 351 (1972).

[9] W. A. Phillips, Rep. Prog. Phys. **50**, 1657 (1987).

[10] K. S. Gilroy and W. A. Phillips, Philos. Mag. B **43**, 735 (1981).

[11] G. M. Harry, M. R. Abernathy, A. E. Becerra-Toledo, H. Armandula, E. Black, K. Dooley, M. Eichenfield, C. Nwabugwu, A. Villar, D. R. M. Crooks *et al.*, Class. Quantum Grav. **24**, 405 (2007).

[12] X. Liu, D. R. Queen, T. H. Metcalf, J. E. Karel, and F. Hellman, Phys. Rev. Lett. **113**, 025503 (2014).

[13] M. Molina-Ruiz, Y. J. Rosen, H. C. Jacks, M. R. Abernathy, T. H. Metcalf, X. Liu, J. L. DuBois, and F. Hellman, Phys. Rev. Mater. **5**, 035601 (2021).

[14] G. Vajente, R. Birney, A. Ananyeva, S. Angelova, R. Asselin, B. Baloukas, R. Bassiri, G. Billingsley, M. M. Fejer, D. Gibson *et al.*, Class. Quantum Grav. **35**, 075001 (2018).

[15] I. W. Martin, R. Bassiri, R. Nawrodt, M. M. Fejer, A. Gretarsson, E. Gustafson, G. Harry, J. Hough, I. MacLaren, S. Penn *et al.*, Class. Quantum Grav. **27**, 225020 (2010).

[16] C. Comtet, D. Forest, P. Ganau, G. M. Harry, J. Mackowski, C. Michel, J. Montorio, N. Morgado, V. Pierro, L. Pinard, I. Pinto, and A. Remillieux, in *42nd Rencontres de Moriond on Gravitational Waves and Experimental Gravity* (La Thuile, Italy, 2007).

[17] R. Flaminio, J. Franc, C. Michel, N. Morgado, L. Pinard, and B. Sassolas, Class. Quantum Grav. **27**, 084030 (2010).

[18] T. Li, F. A. Aguilar Sandoval, M. Geitner, L. Bellon, G. Cagnoli, J. Degallaix, V. Dolique, R. Flaminio, D. Forest, M. Granata, C. Michel, N. Morgado, and L. Pinard, Phys. Rev. D **89**, 092004 (2014).

[19] M. Granata, A. Amato, L. Balzarini, M. Canepa, J. Degallaix, D. Forest, V. Dolique, L. Mereni, C. Michel, L. Pinard, B. Sassolas, J. Teillon, and G. Cagnoli, Class. Quantum Grav. **37**, 095004 (2020).

[20] See Supplemental Material at http://link.aps.org/supplemental/10.1103/PhysRevMaterials.8.035603 for details on the composition of a-Ta_2O_5 films, which includes Ref. [21].

[21] N. Banno, T. Sakamoto, N. Iguchi, M. Matsumoto, H. Imai, T. Ichihashi, S. Fujieda, K. Tanaka, S. Watanabe, S. Yamaguchi, T. Hasegawa, and M. Aono, Appl. Phys. Lett. **97**, 113507 (2010).

[22] G. G. Stoney, Proc. Royal Soc. A **82**, 172 (1909).

[23] C. A. Klein, J. Appl. Phys. **88**, 5487 (2000).

[24] C.-L. Tien, C.-C. Lee, K.-P. Chuang, and C.-C. Jaing, J. Mod. Opt. **47**, 1681 (2000).

[25] T. Middelmann, A. Walkov, G. Bartl, and R. Schödel, Phys. Rev. B **92**, 174113 (2015).

[26] A. S. Ferlauto, G. M. Ferreira, J. M. Pearce, C. R. Wronski, R. W. Collins, X. Deng, and G. Ganguly, J. Appl. Phys. **92**, 2424 (2002).

[27] X. Liu and R. O. Pohl, Phys. Rev. B **58**, 9067 (1998).
[28] T. H. Metcalf, X. Liu, and M. R. Abernathy, J. Appl. Phys. **123**, 235105 (2018).
[29] C. L. Spiel, R. O. Pohl, and A. T. Zehnder, Rev. Sci. Instrum. **72**, 1482 (2001).
[30] X. Liu, S. F. Morse, J. F. Vignola, D. M. Photiadis, A. Sarkissian, M. H. Marcus, and B. H. Houston, Appl. Phys. Lett. **78**, 1346 (2001).
[31] E. Cesarini, M. Lorenzini, E. Campagna, F. Martelli, F. Piergiovanni, F. Vetrano, G. Losurdo, and G. Cagnoli, Rev. Sci. Instrum. **80**, 053904 (2009).
[32] G. Vajente, A. Ananyeva, G. Billingsley, E. Gustafson, A. Heptonstall, E. Sanchez, and C. Torrie, Rev. Sci. Instrum. **88**, 073901 (2017).
[33] R. Bassiri, K. B. Borisenko, D. J. H. Cockayne, J. Hough, I. MacLaren, and S. Rowan, Appl. Phys. Lett. **98**, 031904 (2011).
[34] A. Amato, M. Magnozzi, N. Shcheblanov, A. Lemaître, G. Cagnoli, M. Granata, C. Michel, G. Gemme, L. Pinard, and M. Canepa, ACS Appl. Opt. Mater. **1**, 395 (2023).
[35] D. J. Kalnicky and T. D. Moustakas, Anal. Chem. **53**, 1792 (1981).
[36] K. Kamoshida, Thin Solid Films **283**, 57 (1996).
[37] K. Prasai, K. Lee, B. Baloukas, H.-P. Cheng, M. Fazio, L. Martinu, A. Mehta, C. S. Menoni, F. Schiettekatte, R. Shink, B. Shyam, G. Vajente, M. M. Fejer, and R. Bassiri, APL Mater. **11**, (2023).
[38] R. Bassiri, K. B. Borisenko, I. MacLaren, J. Hough, D. J. H. Cockayne, and S. Rowan, J. Phys.: Conf. Ser. **241**, 012070 (2010).
[39] T. Damart, E. Coillet, A. Tanguy, and D. Rodney, J. Appl. Phys. **119**, 175106 (2016).
[40] C. Joseph, P. Bourson, and M. D. Fontana, J. Raman Spectrosc. **43**, 1146 (2012).
[41] A. L. Gubskil, A. P. Kovtun, and S. D. Khanin, Sov. Phys. Solid State **29**, 611 (1987).
[42] P. S. Dobal, R. S. Katiyar, Y. Jiang, R. Guo, and A. S. Bhalla, J. Raman Spectrosc. **31**, 1061 (2000).
[43] B. Shyam, K. H. Stone, R. Bassiri, M. M. Fejer, M. F. Toney, and A. Mehta, Sci. Rep. **6**, 32170 (2016).
[44] R. M. Fleming, D. V. Lang, C. D. W. Jones, M. L. Steigerwald, D. W. Murphy, G. B. Alers, Y.-H. Wong, R. B. van Dover, J. R. Kwo, and A. M. Sergent, J. Appl. Phys. **88**, 850 (2000).
[45] A. Amato, S. Terreni, M. Granata, C. Michel, B. Sassolas, L. Pinard, M. Canepa, and G. Cagnoli, Sci. Rep. **10**, 1670 (2020).
[46] M. Cevro, Thin Solid Films **258**, 91 (1995).
[47] A. Amato, S. Terreni, V. Dolique, D. Forest, G. Gemme, M. Granata, L. Mereni, C. Michel, L. Pinard, B. Sassolas, J. Teillon, G. Cagnoli, and M. Canepa, J. Phys. Mater. **2**, 035004 (2019).
[48] S. Rau, C. Enss, S. Hunklinger, P. Neu, and A. Würger, Phys. Rev. B **52**, 7179 (1995).
[49] M. A. Fazio, G. Vajente, A. Ananyeva, A. Markosyan, R. Bassiri, M. M. Fejer, and C. S. Menoni, Opt. Mater. Express **10**, 1687 (2020).
[50] A. Foroughi-Abari, C. Xu, and K. C. Cadien, Thin Solid Films **520**, 1762 (2012).
[51] E. A. Ellis, M. Chmielus, and S. P. Baker, Acta Mater. **150**, 317 (2018).
[52] M. D. Ediger, J. Chem. Phys. **147**, 210901 (2017).
[53] K. Prasai, R. Bassiri, H.-P. Cheng, and M. M. Fejer, Phys. Status Solidi B **258**, 2000519 (2021).
[54] K. Prasai, J. Jiang, A. Mishkin, B. Shyam, S. Angelova, R. Birney, D.A. Drabold, M. Fazio, E.K. Gustafson, G. Harry, S. Hoback, J. Hough, C. Levesque, I. MacLaren, A. Markosyan, I.W. Martin, C.S. Menoni, P.G. Murray, S. Penn, S. Reid, R. Robie, S. Rowan, F. Schiettekatte, R. Shink, A. Turner, G. Vajente, H.P. Cheng, M.M. Fejer, A. Mehta, and R. Bassiri, Phys. Rev. Lett. **123**, 045501 (2019).
[55] Y. Kim, S. Cho, Y. Seo, H. Yoon, Y. Im, and D. Yoon, Cryst. Res. Technol. **37**, 1257 (2002).
[56] M. Granata, E. Coillet, V. Martinez, V. Dolique, A. Amato, M. Canepa, J. Margueritat, C. Martinet, A. Mermet, C. Michel, L. Pinard, B. Sassolas, and G. Cagnoli, Phys. Rev. Mater. **2**, 053607 (2018).
[57] M. A. Fazio, G. Vajente, L. Yang, A. Ananyeva, and C. S. Menoni, Phys. Rev. D **105**, 102008 (2022).
[58] X. Liu, M. R. Abernathy, T. H. Metcalf, B. Jugdersuren, J. C. Culbertson, M. Molina-Ruiz, and F. Hellman, J. Alloys Compd. **855**, 157431 (2021).
[59] T. H. Metcalf, X. Liu, G. Jernigan, J. C. Culbertson, M. Abernathy, M. Molina-Ruiz, and F. Hellman, J. Alloys Compd. **856**, 157616 (2021).